ACS OMEGA

http://pubs.acs.org/journal/acsodf

Article

Enhancing the Phosphate Adsorption of a Polyallylamine Resin in Alkaline Environments by Lanthanum Oxalate Modification

Xiaofeng Xu, Ruonan Li, Jinglin Chen, Jie Yang, Yukai Wu, Junrui Liu, You-gui Huang, Shaohua Chen, Xin Ye,* and Wei Wang*

Cite This: *ACS Omega* 2022, 7, 19743−19753

Read Online

ACCESS | Metrics & More | Article Recommendations | Supporting Information

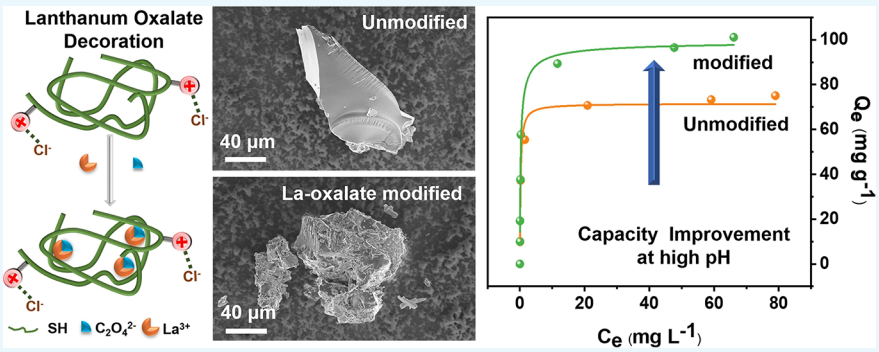

ABSTRACT: Sevelamer hydrochloride (SH), originally developed as an oral pharmaceutical for controlling blood phosphate levels, is a polyallylamine resin that could be used in water treatments. Although it binds phosphates effectively, its adsorption capacity suffers from a significant loss at high pH. Here, we modify SH with lanthanum oxalate to improve its phosphate adsorption in alkaline environments. With less than 6.00 wt% in La content, the composite adsorbent (SH-1C-1La) exhibits an adsorption capacity of 109.3 mg P g^{-1} at pH 8.0 and 100.2 mg P g^{-1} at pH 10.0, demonstrating significant enhancement from the original SH (86.3 mg P g^{-1} at pH 8.0 and 69.4 mg P g^{-1} at pH 10.0). Besides its high adsorption capacity and rapid adsorption kinetics, SH-1C-1La is capable of maintaining more than 78% of its capacity after four regeneration cycles, showing good durability in long-term applications. Zeta-potential measurements and XPS analysis reveal that the lanthanum oxalate species increase the surface potential to enhance the electrostatic adsorption while introducing chemical binding sites for phosphate ions. Both factors lead to the improved adsorption properties. The modification by lanthanum oxalate species might provide a new alternative for improving the phosphate adsorption properties of anion-exchange resins.

1. INTRODUCTION

Phosphorus (P) is a basic element of life and exists most commonly as phosphate ions in aqueous environments.[1] Generally, autotrophic organisms only adsorb phosphorus as phosphates, making phosphate fertilization a significant factor in plant growth and crop productions.[2,3] However, with the booming population, the ever-increasing agriculture scale leads to largely excessive phosphate discharge into the environment, causing adverse effects on the ecosystem. For example, eutrophication induced by high phosphorus content results in the well-known algae bloom, which consumes the dissolved oxygen and causes the mass death of aquatic lives.[4] Therefore, it is of great importance to control the phosphate level before discharging.

Anion-exchange resins are a group of materials that are often used to adsorb phosphates in water.[5,6] The framework of anion-exchange resins consists of hydrocarbon backbones, forming a three-dimensional network after cross-linking. With cationic functional groups anchored on the backbone, the anion-exchange resin stores charge-balancing anions that could exchange with the anion species in water.[7] For instance, D201 is a strong base anion-exchange resin widely used in pollutant removal. Its phosphate adsorption mainly proceeds by the electrostatic force between the quaternary amine groups and phosphate ions, through exchanging with the stored Cl^- ions.[8] However, despite its wide application, D201's adsorption capacity for phosphorus is limited (i.e., 16.3 mg P g^{-1} at the phosphorus concentration of 10 mg P L^{-1}), with the adsorption equilibrium slowly reached in 6 h.[9] Additionally, the common anion-exchange resins are mostly applied in acidic or neutral environments. As the pH increases above 7, the

Received: March 14, 2022
Accepted: May 16, 2022
Published: May 28, 2022

anion-exchange resins will gradually translate into the charge-neutral form, which shows limited adsorption for oxyanions.[10] Wrong et al. explain that the free base form of resin losses the ion exchange function and could not bind phosphate at high pH, which limits their application in alkaline conditions.[11]

Sevelamer hydrochloric is an anion-exchange resin in the chloride form, exhibiting high phosphate adsorption capacity because of its high density of functional groups.[12] It is originally developed to remove the excess serum phosphate in patients who are diagnosed with end-stage renal disease (ESRD).[13] The phosphate binding of SH is mainly through physical adsorption, such as ion exchange and hydrogen bonding.[14−17] With its high density of amine groups, SH exhibits rapid phosphate adsorption and large capacity.[14] The hydrogen bonding from multiple amine groups also greatly improves the selectivity for phosphate adsorption.[10,18] Currently, there are more and more research focusing on further improving the adsorption characteristics of SH because its patent expired in 2014.[16,17] Nevertheless, the common disadvantage of anion-exchange resins exists in SH, rendering its adsorption performance decreasing dramatically at high pH. In an alkaline environment, the amine groups will be deprotonated, leading to the quickly declined adsorption capacity.[10,11,14,15] With the potential of being applied in water treatments, it would be important to modify SH for maintaining high phosphate adsorption under alkaline conditions.

It is known that the metal oxide/hydroxide materials adsorb phosphate ions through ligand exchange to form inner-sphere complexation, which can proceed even in alkaline environments.[19,20] Over recent years, lanthanum has received widespread attention because of its moderately abundant reserves, low toxicity, and great affinity for binding phosphates.[21,22] Current examples include compositing lanthanum compounds (e.g., $La(OH)_3$) with supporting matrixes (e.g., carbon nanotubes, biochar, or anion-exchange resins).[5,23−25] However, simply transferring this strategy may not be suitable for modifying SH. The reasons are mainly twofold. First, the synthesis of $La(OH)_3$ requires the use of a strong basic compound, such as NaOH, which causes deprotonation of amine functional groups and therefore may significantly reduce the intrinsic adsorption property of SH. Reprotonation can only be carried out in an acidic environment, which inevitably leads to the dissolution of lanthanum components. Second, with metal oxide/hydroxide as the major adsorbing component, the regeneration of the adsorbent may be more challenging.[20]

In this study, we synthesize a series of composite adsorbents (SH-C-La) consisting of lanthanum oxalate and SH, aiming for improving the adsorption property of SH in an alkaline environment. As a lanthanum-containing compound, the synthesis of lanthanum oxalate does not require basic conditions, which avoids deprotonating the amine groups on SH. The synthetic process is carefully tuned to maintain the properties of SH, for rapid adsorption and facile regeneration. To further investigate the adsorption behavior of SH-C-La samples, a series of adsorption characterizations are conducted, including pH stability, adsorption selectivity, adsorption isotherm, and adsorption kinetics. The mechanism for P adsorption is studied by X-ray diffraction (XRD), Fourier transform infrared (FT-IR), scanning electron microscopy−energy-dispersive X-ray spectroscopy (SEM-EDS), inductively coupled plasma-optical emission spectroscopy (ICP-OES), and X-ray photoelectron spectroscopy (XPS), to explain the effect of lanthanum oxalate on the adsorption characteristics of SH.

2. MATERIALS AND METHODS

2.1. Chemicals. All chemicals used in this study were of analytical grade. $LaCl_3{\cdot}7H_2O$ and $H_2C_2O_4{\cdot}2H_2O$ were purchased from Adamas. KH_2PO_4, Na_2CO_3, NaOH, $NaHCO_3$, and NaCl were obtained from General Reagent. SH was supplied by Hangzhou Bingochem Co. Ltd.

2.2. Synthesis of Lanthanum Oxalate-Modified SH. SH (0.5 g) was dispersed in 20 mL of 2.5 mmol L^{-1} $H_2C_2O_4$ aqueous solution and stirred at room temperature for 12 h. The solid material was then separated by filtration and added to 20 mL of 100 mmol L^{-1} $LaCl_3$ solution for another 12 h of stirring. During this process, the La ions react with the preloaded oxalate to form precipitation. After the reaction, the materials were filtered and washed thoroughly with deionized water to remove the residual ions. The solid product was vacuum-dried at 105 °C for 12 h and named "SH-0.025C-1La" according to the molar ratio between $C_2O_4^{2-}$ and La^{3+} (the C/La ratio) in the synthesis.

To investigate the effect of $H_2C_2O_4$ concentration on the adsorbent properties, we fixed the $LaCl_3$ concentration at 100 mmol L^{-1} and varied the concentration of $H_2C_2O_4$ to 5, 25, 50, and 250 mmol L^{-1}, corresponding to the C/La ratios of 0.05:1, 0.25:1, 0.5:1, and 2.5:1. The as-obtained samples were denoted as SH-0.05C-1La, SH-0.25C-1La, SH-0.5C-1La, and SH-2.5C-1La, respectively.

On the other hand, to investigate the concentration effect of La^{3+} solution, the $H_2C_2O_4$ concentration was set to 25 mmol L^{-1} when the La^{3+} solution of different concentrations (15, 25, 50, 100, and 200 mmol L^{-1}) was added. The corresponding products were named SH-1C-0.6La, SH-1C-1La, SH-1C-2La, SH-1C-4La, and SH-1C-8La based on the ratio between the $C_2O_4^{2-}$ and La^{3+}.

For comparison, lanthanum oxalate (La-oxalate) was prepared by reacting 20 mL of 25 mmol L^{-1} $H_2C_2O_4$ solution with 20 mL of 25 mmol L^{-1} $LaCl_3$ solution. The solid product was filtered, washed thoroughly with DI water, and then vacuum-dried at 105 °C for 12 h.

2.3. Material Characterization. The crystallographic information of the samples was obtained by XRD using a powder X-ray diffractometer (Miniflex 600, Japan) equipped with Cu Kα radiation (40 kV, 15 mA). The XRD patterns were collected in the two-theta range of 5−60° with a scan rate of 5°/min. FT-IR spectra were recorded on a Nicolet iS 50 (Thermo Fisher, USA) in the range 500−4000 cm^{-1} at room temperature by averaging 16 scans. The morphology and elemental distribution of the samples were characterized by a SEM (Apreo, S LoVac, Czech Republic) instrument equipped with an EDS attachment. To test the La leaching of the adsorbent, ICP-OES (ULTIMA 2, France) was used to determine the La concentration in the solution after the adsorption process. The zeta-potential was measured using a multiangle particle size and a high-sensitivity zeta-potential analyzer (Omni, Brookhaven). During the Zeta-potential measurement, the pH was adjusted between 2.0 and 11.0 by adding 100 mmol L^{-1} NaOH or 100 mmol L^{-1} HCl aqueous solutions. XPS (AXIS SUPRA, Kratos, UK) was carried out with the Al Kα anode radiation (ν = 1486.6 eV, 150 W) as the X-ray source. The binding energy values were referenced to the C 1s peak at 284.8 eV, and the experimental data were analyzed by the XPSPeak41 software.

https://doi.org/10.1021/acsomega.2c01520
ACS Omega 2022, 7, 19743−19753

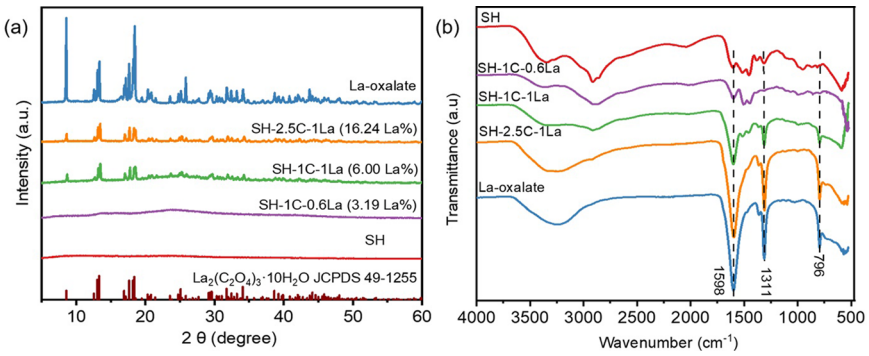

Figure 1. XRD patterns of SH, SH-1C-0.6La (3.19% La), SH-1C-1La (6.00% La), SH-2.5C-1La (16.24% La), and La-oxalate (a); FT-IR spectra of SH, SH-1C-0.6La, SH-1C-1La, SH-2.5C-1La, and La-oxalate (b).

2.4. Static Adsorption Experiment. The traditional bottle-point method was used to study the static adsorption properties, where 0.50 g L^{-1} adsorbent was used in all static adsorption experiments. The adsorption process was performed in a 150 mL flask with 100 mL of phosphate solution (100 mg P L^{-1}) for 2 h to reach the adsorption equilibrium. During the process, the flask was placed in an incubator shaker (HY-5S, Shanghai Huaying) at 180 rpm (25 °C).

After adsorption, we used the antimony-molybdate reaction with ascorbic acid to determine the residual *P* concentrations in solution.[26] The equilibrium adsorption capacity, Q_e (mg P g^{-1}), was determined using eq 1:

$$Q_e = \frac{(C_0 - C_e)}{m} V \quad (1)$$

where C_0 is the initial *P* concentration (mg P L^{-1}), C_e is the residual concentration (mg P L^{-1}), *V* is the volume of solution (L), and *m* is the adsorbent mass (g).

2.4.1. Evaluation of the pH Stability and Selectivity of the Adsorbent. To evaluate the phosphate adsorption capacity at different pH, the pH of the phosphate-containing solution (100 mg P L^{-1}) was adjusted from 2.0 to 11.0 by 100 mmol L^{-1} HCl or 100 mmol L^{-1} NaOH before static adsorption measurements. The equilibrium adsorption capacity of the adsorbent and La leaching were determined after the static adsorption experiment.

The effect of coexisting ions was tested by adding each of the following compounds: NaCl, Na_2SO_4, $NaNO_3$, Na_2CO_3, and humic acid (as A^-) to the phosphate-containing solution (100 mg P L^{-1}). The molar ratio between the competing ion and the phosphate ion was set to 1:1. Static adsorption experiments were conducted to evaluate the equilibrium adsorption capacity of the adsorbent in these solutions. To explore the adsorption under alkaline conditions, the experiments were performed at pH 8.0 and 10.0.

2.4.2. Adsorption Kinetic and Isotherm Measurements. To measure the adsorption isotherms, static adsorption experiments were conducted with 100 mL solution of different initial *P* concentrations, such as 0, 5, 10, 20, 30, 60, 100, and 120 mg L^{-1}, with 0.50 g L^{-1} adsorbents at pH 8.0 and 10.0. The reaction time was set to 2 h, with the operation temperature of 25 °C. The obtained isotherms were fitted by Langmuir and Freundlich isotherm models.

The Langmuir model can be described as follows (eq 2):

$$Q_e = \frac{Q_m K_L C_e}{1 + K_L C_e} \quad (2)$$

where Q_e (mg g^{-1}) is the equilibrium adsorption capacity, Q_m (mg g^{-1}) is the maximum adsorption capacity, K_L (L mg^{-1}) is the Langmuir isotherm content, and C_e (mg L^{-1}) is the equilibrium concentration of the phosphate ion.

The Freundlich model can be described as eq 3:

$$Q_e = K_F C_e^{1/n} \quad (3)$$

where Q_e (mg g^{-1}) is the equilibrium adsorption capacity, C_e (mg L^{-1}) is the equilibrium concentration of phosphate, and K_F (mg g^{-1}) is the Freundlich isotherm content. Here, $1/n$ is a parameter representing the strength of adsorption: the adsorption becomes stronger with decreasing $1/n$ values.

Kinetic studies were conducted using 250 mg of adsorbents in 500 mL of phosphate solution (100 mg P L^{-1}) at two different pH values (8.0 and 10.0). The supernatant (1 mL) was taken at various time intervals (5−480 min) to determine the *P* concentration.

The pseudo-first-order model (eq 4) and pseudo-second-order model (eq 5) were used to fit kinetic curves:

$$Q_t = Q_e(1 - e^{k_1 t}) \quad (4)$$

$$Q_t = \frac{k_2 Q_e^2 t}{1 + k_2 Q_e t} \quad (5)$$

where Q_t (mg g^{-1}) represents the adsorption capacity at time *t* (min), and Q_e (mg g^{-1}) is the adsorption capacity at equilibrium. Furthermore, k_1 (min $^{-1}$) is the pseudo-first-order rate constant and k_2 (g mg^{-1} min^{-1}) is the pseudo-second-order rate constant.

2.5. Regeneration Experiments. The regeneration of the SH-C-La samples was conducted by dispersing 1.0 g of the exhausted adsorbent into 100 mL of solution containing 1.0 mol L^{-1} $H_2C_2O_4$ and 2.0 mol L^{-1} NaCl. The mixture was heated at 60 °C and stirred at 800 rpm for 12 h. After stirring, the adsorbent was filtered and rinsed thoroughly with deionized water. Finally, the regenerated samples were vacuum-dried for 12 h before application.

For regenerated samples, the regeneration efficiency (R_e, %) was calculated from eq 6:

$$R_e(\%) = \frac{Q_n}{Q_e} \quad (6)$$

where Q_n (mg P g^{-1}) is the phosphate adsorption capacity after the *n*th regeneration. For example, Q_1 (mg P g^{-1}) is the adsorption capacity after the first regeneration.

https://doi.org/10.1021/acsomega.2c01520
ACS Omega 2022, 7, 19743−19753

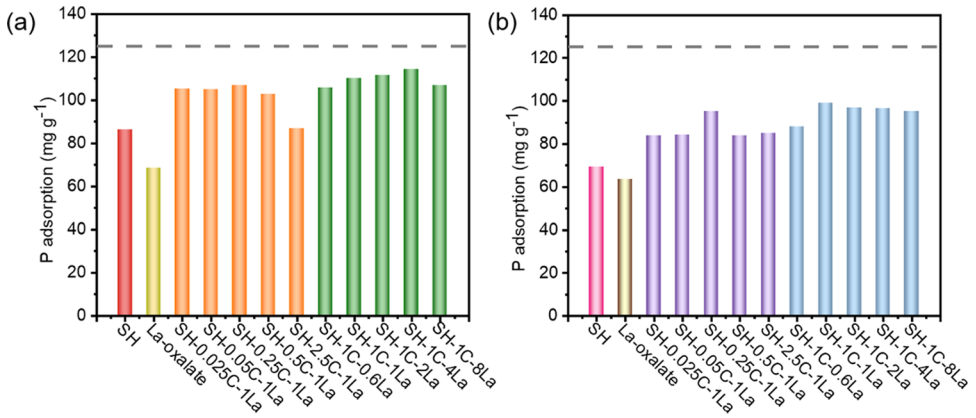

Figure 2. *P* adsorption capacity values of various as-prepared adsorbents at pH 8.0 (a) and pH 10.0 (b). The dashed line represents the adsorption value of SH at pH 7.0.

3. RESULTS AND DISCUSSION

3.1. Characterization of the Adsorbents. According to the stoichiometry of lanthanum oxalate (La^{3+}:$C_2O_4^{2-}$ = 2:3), we adopt a series of different C/La ratios (from 0.025 to 2.5) during the synthesis to obtain different compositions. To verify the successful synthesis of the targeted composites, we use a suite of techniques including ICP-OES, XRD, FT-IR, and SEM-EDS to characterize different samples. Table S1 lists the La loading (in wt%) of various as-prepared SH-C-La samples by ICP-OES measurements. We find that SH-1C-0.6La contains the lowest La loading of 3.19% while SH-2.5C-1La contains the highest La loading of 16.24%. The La loading of other samples falls in between, for example, 6.00% for SH-1C-1La.

The XRD patterns of SH, SH-1C-0.6La, SH-1C-1La, SH-2.5C-1La, and La-oxalate are shown in Figure 1a. As we can see, La-oxalate exhibits a diffraction pattern consistent with the monoclinic $La_2(C_2O_4)_3{\cdot}10H_2O$ (JCPDS 49-1255).[27,28] SH and SH-1C-0.6La are amorphous according to the XRD patterns, because no or low La loading is associated with these two samples. In contrast, SH-1C-1La and SH-2.5C-1La exhibit diffraction patterns that are similar to La-oxalate but with lower diffraction intensity. This demonstrates that $La_2(C_2O_4)_3{\cdot}10H_2O$ is successfully composited with the SH matrix in samples such as SH-1C-1La and SH-2.5C-1La.

FT-IR spectra are collected to analyze the functional groups on SH, SH-1C-0.6La, SH-1C-1La, SH-2.5C-1La, and La-oxalate (Figure 1b). SH exhibits the characteristic N−H stretching vibration (3344 cm^{-1}) and N−H bending vibration (1603 cm^{-1}).[29] The absorption peaks at 2921 and 1452 cm^{-1} belong to the asymmetric stretching vibration and the bending vibration, respectively, of $-CH_2$ groups.[30] For La-oxalate, the FT-IR spectrum first presents a broad peak at 3237 cm^{-1}, which can be assigned to the stretching vibration of −OH. Next, the two sharp peaks at 1598 and 1311 cm^{-1} are attributed to the −C═O and C−O vibration, originated from the $C_2O_4^{2-}$ groups. Another intense signal at 796 cm^{-1} is likely caused by the stretching vibration of La−O.[27,28]

After the lanthanum oxalate modification, SH-1C-0.6La exhibits similar signals compared to SH, which is again consistent with its low La loading. On the other hand, the FT-IR signals of SH-1C-1La and SH-2.5C-1La possess the characteristics of both SH and La-oxalate, but with lower intensity. This also confirms the successful synthesis of targeted composites.

The surface morphologies of SH, SH-1C-0.6La, SH-1C-1La, SH-2.5C-1La, and La-oxalate are studied by SEM. For SH, the SEM image (Figure S1a) shows its bulklike morphology with a smooth surface. La-oxalate particles, on the other hand, shows prismlike structures similar to the previous studies (Figure S2).[27,28] After the lanthanum oxalate modification, different amounts of lanthanum oxalate particles appear on the surface of SH (Figure S1b−S1d). The surface of SH-1C-0.6La (Figure S1b) possesses very few particles, which further supports the XRD and FT-IR observations of low La loading. With the increasing La loading, improved particle coverage could be observed on the surface of SH blocks. Compared to SH-1C-1La (Figure S1c), the surface of SH-2.5C-1La is covered with prismlike particles in a much higher density (Figure S1d). Compositional analysis is conducted on SH-1C-1La by EDS line scanning (Figure S3). Both of the La and O signals are detected when scanning across the prismlike particles, confirming that the attached particles are indeed lanthanum oxalate.

3.2. Characterization of the Adsorption Capacity. Because we aim to improve the alkaline adsorption of SH, it is important to determine at which condition we shall measure the static adsorption capacity. Figure S4 illustrates the P adsorption capacity of SH at various pH values (2−11). It is clear that the adsorption capacity of SH reaches the maximum value of 153.4 mg P g^{-1} at pH 3.0 and drops sharply in the neutral-alkaline region from 86.3 mg P g^{-1} (pH = 8.0) to 69.4 mg P g^{-1} (pH = 10.0). To directly compare the phosphate adsorption of different samples under alkaline conditions, we decide to conduct static adsorption experiments at pH 8.0 and 10.0 for different SH-C-La samples to determine the optimum composition and the corresponding synthetic conditions.

Figure 2 shows the *P* adsorption capacities (at pH 8.0 and 10.0) of different adsorbents synthesized by varying the oxalic acid concentration. At pH 8.0, compared with SH (86.3 mg P g^{-1}) and La-oxalate (68.53 mg P g^{-1}), the modified samples exhibit increasing capacity with the C/La ratio increasing from 0.025:1 to 0.25:1 (e.g., 107.0 mg P g^{-1} for SH-0.25C-1La). When the C/La ratio continues increasing to 2.5:1 (i.e., 86.7 mg P g^{-1} for SH-2.5C-1La), the adsorption capacity decreases. The excessive lanthanum oxalate deposition may prevent the phosphate ions in the solution from contacting the active sites (Figure S1d). Similarly, at pH 10.0, with the C/La ratio changing from 0.025:1 to 0.25:1, the adsorption capacity increases from 83.9 mg P g^{-1} to 95.1 mg P g^{-1}, significantly

https://doi.org/10.1021/acsomega.2c01520
ACS Omega 2022, 7, 19743−19753

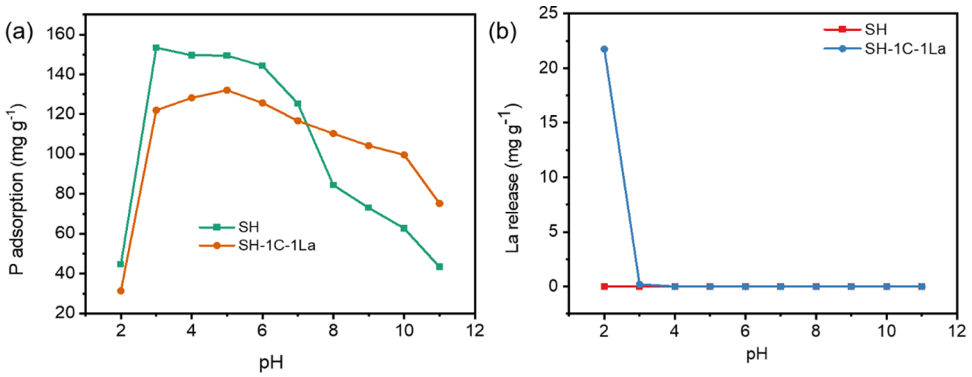

Figure 3. Effect of initial solution pH on the *P* adsorption capacities of SH and SH-1C-1La (a) and the concentration of leaching La^{3+} ions at different pH (b).

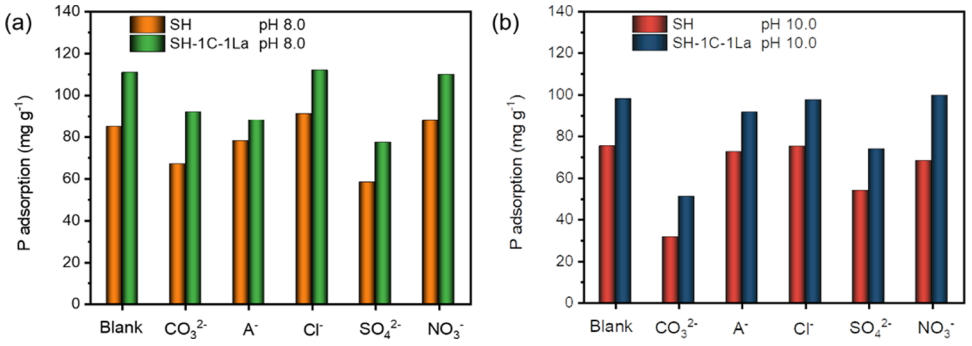

Figure 4. Adsorption capacity of SH and SH-1C-1La in the presence of competing anions at pH 8.0 (a) and pH 10.0 (b).

larger than the pure SH (69.4 mg P g^{-1}) and La-oxalate (63.56 mg P g^{-1}).

To further explore the effect of La^{3+} concentration on the synthesis, we further characterized the adsorption capacity of SH-1C-0.6La, SH-1C-1La, SH-1C-2La, SH-1C-4La, and SH-1C-8La. Overall, the phosphate adsorption capacities of these samples are significantly larger than that of SH. For example, SH-1C-1La exhibits adsorption capacities of 109.3 and 100.2 mg P g^{-1} at pH 8.0 and pH 10.0, respectively. Meanwhile, the adsorption capacity changes slightly between the C/La ratio of 1:1 and 1:4, at both pH values (Figure 2).

Interestingly, when the C/La ratio exceeds 1:12, no precipitation forms on the SH surface. To further investigate the reason for this phenomenon, we leave 5 mL of the synthetic solution on the shelf for ambient evaporation and obtain a lanthanum chloride oxalate trihydrate crystal, the structure of which has been reported by predecessors.[31] It appears that La^{3+} ions mainly exist as $LaCl^{2+}$ in an acid solution with high lanthanum and Cl^- concentrations, which changes the coordination environment and thus produces a soluble structure.[5] Therefore, the concentration of La needs to be controlled within a certain range to achieve the modification.

To achieve a high P adsorption capacity and minimize lanthanum consumption, SH-1C-1La appears to be a good choice. Its C/La ratio is 1:1, with the concentration of $C_2O_4^{2-}$ and La^{3+} both set to 0.025 mol L^{-1} during the synthesis. In the following sections, the properties of SH-1C-1La are comprehensively characterized to compare its adsorption behavior with SH and reveal the mechanism of adsorption enhancement.

3.3. Effect of Initial pH on Static Adsorption. To compare the adsorption properties between SH and SH-1C-1La, we characterize their static adsorption capacities in various pH values (2.0∼11.0), as shown in Figure 3a. At the pH range of 2.0∼7.0, although SH-1C-1La exhibits lower adsorption capacity than SH, all measured capacity values are larger than 120 mg P g^{-1}, which are high among the reported adsorbents.[20] When the pH keeps increasing and the solution becomes basic, SH-1C-1La shows improved adsorption capacity compared with pure SH (e.g., the adsorption captaincy values of SH-1C-1La are 109.3 and 100.2 mg P g^{-1} at pH 8.0 and 10.0, respectively). We plot the ratio between static adsorption capacities of SH-1C-1La and pure SH (Figure S5). As a result, the adsorption enhancement effect increases with the increasing pH.

Meanwhile, the La leaching of SH-1C-1La at different pH is also characterized. From Figure 3b, we observe that the La leaching only happens at a pH lower than 3.0 because the excess hydrogen ions can dissolve the lanthanum oxalate. At a pH above 3.0, SH-1C-1La is stable without observable La leaching. This makes SH-1C-1La suitable for applications in treating natural water reservoirs (typically with pH above 6.0).

3.4. Effect of Competing Ions on the Phosphate Adsorption. In water treatment processes, various anions may exist and interfere with the adsorption of phosphate. Common anions, such as CO_3^{2-}, SO_4^{2-}, NO_3^-, Cl^-, and A^- (humic acid anions), are typically chosen as the competing anions to explore the selectivity of adsorbents for phosphate adsorption.[5,32] As we can see, at pH 8.0, in spite of the presence of Cl^- and NO_3^-, the P adsorption of SH and SH-1C-1La remains uninfluenced (Figure 4a). This could be expected because the monovalent ions (Cl^- and NO_3^-) have a lower charge than phosphate ions and therefore do not compete effectively for electrostatic interactions. On the other hand,

https://doi.org/10.1021/acsomega.2c01520
ACS Omega 2022, 7, 19743−19753

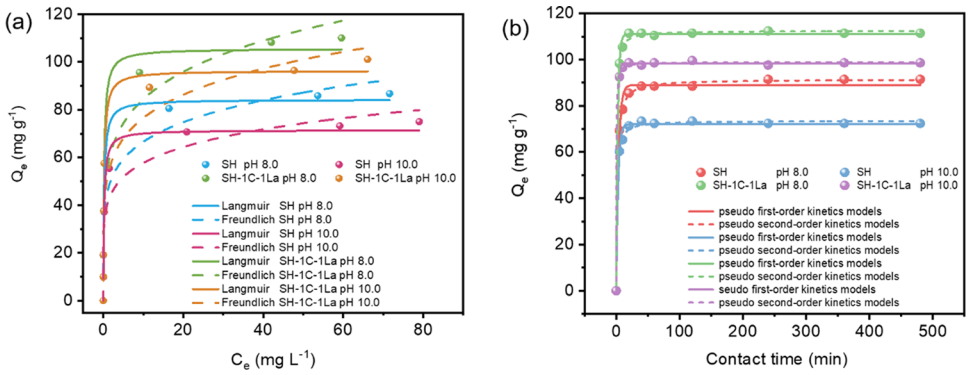

Figure 5. Adsorption isotherms of SH and SH-1C-1La at pH 8.0 and 10.0 with Langmuir and Freundlich model fittings (a); adsorption kinetic data of SH and SH-1C-1La with pseudo first-order and pseudo-second-order kinetics fittings (b).

Table 1. Adsorption Isotherm Parameters for Langmuir and Freundlich Models

		Langmuir model				Freundlich model		
	pH	Q_m mg g^{-1}	K_L L mg^{-1}	R_L	R^2	K_F mg g^{-1}	$1/n$	R^2
SH	8	84.29	4.55	0.0036	0.988	45.24	0.16	0.919
SH	10	71.50	4.77	0.0035	0.969	40.16	0.16	0.925
SH-1C-1La	8	105.62	4.79	0.0035	0.982	55.22	0.18	0.946
SH-1C-1La	10	96.38	4.75	0.0035	0.976	51.44	0.17	0.937

CO_3^{2-} and SO_4^{2-} affect phosphate adsorption on both SH and SH-1C-1La at pH 8.0. These divalent ions (CO_3^{2-} and SO_4^{2-}) have high negative charge densities capable of competing with phosphate for the active sites.[33] Nevertheless, it is worth noticing that under the interference by the same divalent ions (CO_3^{2-} or SO_4^{2-}), SH-1C-1La exhibits higher phosphate adsorption than SH (i.e., the adsorption capacities of SH-1C-1La are 91.7 and 77.3 mg P g^{-1} in the presence of CO_3^{2-} and SO_4^{2-}, respectively). Finally, the effect by A^- is somewhere between the monovalent and divalent anions. It appears that A^- might have more effect on SH-1C-1La than SH, which could be ascribed to the formation of complexes between A^- and La^{3+}.[34]

When the pH increases to 10.0, the overall trend remains similar (Figure 4b). Under the existence of CO_3^{2-}, the adsorption capacity of both samples suffers a greater loss than the situation at pH 8.0. The reason might be that the CO_3^{2-}, in equilibration with HCO_3^- to a much less extent at this pH, is more competitive in occupying the active sites.[35] The increasing valence of the competing ions will also decrease the adsorption density on the adsorbent.[32] The same negative effect can also be observed in the presence of SO_4^{2-}. However, in both cases (with CO_3^{2-} and SO_4^{2-}), SH-1C-1La again exhibits a larger adsorption capacity than SH. For example, with SO_4^{2-} as the competing ion, the adsorption capacity of SH-1C-1La is 73.9 mg P g^{-1}, while that of SH is 54.0 mg P g^{-1}.

Overall, SH-1C-1La exhibits similar *P* adsorption selectivity as SH but exhibits higher adsorption capacity at all conditions. With similar selectivity, SH-1C-1La is capable of removing more phosphate ions than SH, which could also be considered as an improvement on adsorption behavior in the presence of competing ions.

3.5. Adsorption Isotherm. To further investigate the P adsorption behavior of SH and SH-1C-1La, batch adsorption experiments are conducted with different phosphate concentrations (Figure 5a). As we can see, the adsorption capacities of both adsorbents increase rapidly with the initial *P* concentration and reach maximum adsorption at the equilibrium concentration of 60 mg L^{-1} (corresponding to the initial *P* concentration of 100 mg L^{-1}). The adsorption isotherms of SH and SH-1C-1La at different pH are fitted with the Langmuir and the Freundlich isotherm models to study the adsorption behaviors.[36] The fitting parameters are listed in Table 1.

Comparing the regression coefficient (R^2) of the two models, the Langmuir model demonstrates a better fit for SH and SH-1C-1La at both pH. The maximum theoretical adsorption value of SH-1C-1La at pH 8.0 and 10.0 are 105.6 and 96.4 mg P g^{-1}, respectively, based on the Langmuir model. They are more consistent with the experimental data (e.g., 109.3 mg P L^{-1} at pH 8.0 and 100.2 mg P L^{-1} at pH 10.0) than THE Freundlich isotherm model. In addition, K_L in the Langmuir isotherm model represents the strength of interactions between the adsorbent and the adsorbate, and higher values of K_L imply stronger adsorption. The K_L values of both adsorbents exceed 4.5 L mg^{-1}, which may explain the high capacities for adsorbing phosphate ions. The Langmuir isotherm model indicates that the adsorption on both adsorbents is likely a monolayer type, with the active sites homogeneously distributed.[37] Once an adsorption site is occupied, it reaches saturation and cannot accept another adsorbate. This is consistent with the characteristic of the amidocyanogen-rich surface of these adsorbents.[38,39]

In addition, the separation factor (R_L) is typically used to describe the affinity between the adsorbent and the adsorbate. It is a basic parameter of the Langmuir isotherm model, which is defined by eq 7:

$$R_L = \frac{1}{(1 + K_L C_O)} \tag{7}$$

where C_o (mg L^{-1}) is the initial concentration of phosphate ions. The value of R_L implies the adsorption isotherm to be unfavorable ($R_L > 1$), linear ($R_L = 1$), favorable ($0 < R_L < 1$), or irreversible ($R_L = 0$).[38] In Table 1, we find that the R_L values

https://doi.org/10.1021/acsomega.2c01520
ACS Omega 2022, 7, 19743−19753

Table 2. Adsorption Kinetic Fitting by Pseudo First-Order and Pseudo Second-Order Models

		pseudo-first-order			pseudo-second-order		
	pH	K_1 min^{-1}	$Q_{e,1}$ mg g^{-1}	R^2	K_2 g mg^{-1} min^{-1}	$Q_{e,2}$ mg g^{-1}	R^2
SH	8	0.27	88.98	0.990	0.00686	91.42	0.999
SH	10	0.34	72.13	0.993	0.01263	73.53	0.997
SH-1C-1La	8	0.42	111.01	0.998	0.01325	112.48	0.999
SH-1C-1La	10	0.56	98.27	0.999	0.033	98.92	0.999

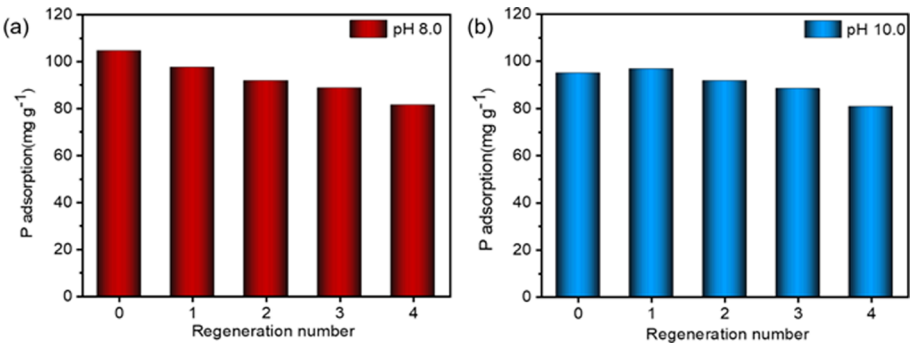

Figure 6. *P* adsorption capacities of SH-1C-1La within four consecutive regeneration cycles at pH 8.0 (a) and pH 10.0 (b).

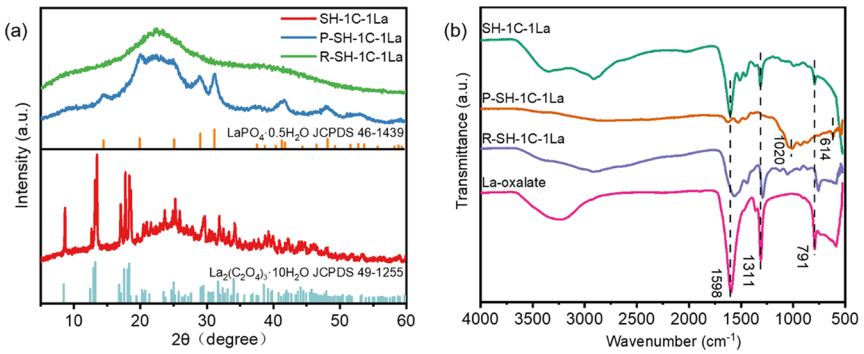

Figure 7. XRD (a) and FT-IR (b) spectra of SH, SH-1C-1La, P-SH-1C-1La, R-SH-1C-1La, and La-oxalate.

are between 0 and 1 in all cases, confirming that the adsorption of phosphates on SH and SH-C-La is favorable.

3.6. Adsorption Kinetics. We measure the adsorption kinetic data of SH and SH-1C-1La (Figure 5b) and use the pseudo-first-order and the pseudo-second-order models[40] to fit the experimental kinetic points (Table 2). It is clear that rapid adsorption happens for both adsorbents. For example, SH-1C-1La reaches adsorption equilibrium within 20 min and SH spends 40 min to reach the equilibrium, both being less than 1 h. According to the kinetic data, pH has little influence on the adsorption rates. It is worth noting that although the correlation coefficient (R^2) of the pseudo-second-order model is slightly higher than that of the pseudo-first-order model, both kinetic models fit well for the adsorbents. This is also reflected by the similar Q_e values provided by the two models. Previous research has indicated that the better fitting by the pseudo-second-order model might stem from its mathematical basis.[41] It may also be why the pseudo-second-order model generally works better among other research.[42] Nevertheless, we need to point out that no matter using which model fitting is performed, the adsorption kinetics remain largely similar before and after the decoration. As a result, the lanthanum oxalate loading effectively increases the adsorption capacity of SH while having little effect on its rapid adsorption behavior.

3.7. Adsorbent Regeneration. The regeneration property is a major factor in evaluating adsorbents for practical applications.[43,44] Because the oxalate acid could desorb the phosphate ions by ligand exchange[45,46] while regenerating lanthanum oxalate species, we use $H_2C_2O_4$ as a major component in the regeneration solution. Figure 6 shows the adsorption capacity of SH-1C-1La after four regeneration cycles (see Table S2 for the regeneration efficiency) at two different pH values. As a result, SH-1C-1La is capable of maintaining more than 78 and 85% of its original capacity after four regeneration cycles at pH 8.0 and 10.0, respectively. It is worth pointing out that after the four regeneration recycles, the La content only decreases by 0.49 wt % (overall) in SH-1C-1La, with low La loading loss each time (Figure S6), again confirming the superior stability of SH-1C-1La. The excellent stability and good regeneration property make SH-1C-1La potentially interesting for water treatment applications.

3.8. Mechanism for Adsorption Enhancement. To explore the mechanism for adsorption enhancement, we need to first investigate the mechanism for phosphate adsorption. The SEM images of the SH-1C-1La after P adsorption (P-SH-1C-1La) are presented in Figure S7. Compared with the original SH-1C-1La, the surface species on P-SH-1C-1La have changed to agglomerated granules of smaller sizes (Figure S7).[47] These granules are identified as $LaPO_4{\cdot}0.5H_2O$ (JCPDS

https://doi.org/10.1021/acsomega.2c01520
ACS Omega 2022, 7, 19743−19753

46-1439) by XRD (Figure 7a), implying that the loading La-oxalate could introduce chemisorption sties and improve the specific binding of phosphate. On the other hand, the EDS mapping indicates the homogeneous distribution of Cl covering the surface of SH-1C-1La, while only P signals can be observed across the entire surface of P-SH-1C-1La (Figure S8). This indicates that the Cl^- in the SH matrix may have been completely exchanged by $H_2PO_4^-$ because of the electrostatic interaction. After *P* adsorption, characteristic peaks appear on the FT-IR spectrum of P-SH-1C-1La at 1020 and 614 cm^{-1}, corresponding to the asymmetric stretching vibrations of P-O and the bending vibration of O−P−O (Figure 7b).[48]

Next, after the first regeneration (sample: R-SH-1C-1La), the XRD pattern changes dramatically (Figure 7a). Unlike SH-1C-1La or P-SH-1C-1La, R-SH-1C-1La is largely amorphous, indicating the loaded lanthanum species has either been dissolved or transformed into other species. Because the lanthanum leaching is small during regeneration (Figure S6), it is likely that the lanthanum components have transformed to other species (either amorphous or nanocrystalline). These species are well-dispersed on the SH matrix but cannot be detected by powder XRD. Meanwhile, we find a redshift on all oxalate-related IR vibrations after the first regeneration (R-SH-1C-1La vs La-oxalate, Figure 7b). The redshift is mainly attributed to the carbonyl group accepting hydrogen bonds from the amine group,[49] instead of binding to La^{3+}. This could imply that the structure of the original La-oxalate changes during the regeneration process. During the regeneration process, the oxalate groups form several hydrogen bonds with the N−H[50] and replace the phosphate ions. Hence, the EDS mapping of the R-SH-1C-1La (first regeneration) shows no P residual (Figure S8), confirming the effective regeneration of SH-1C-1La by oxalic acid-containing solutions.

Because electrostatic interactions are a key driving force for phosphate adsorption on anion-exchange resins, we characterize the zeta potential of different samples. As shown in Figure 8, the zeta potential of all samples, except P-SH, stays relatively

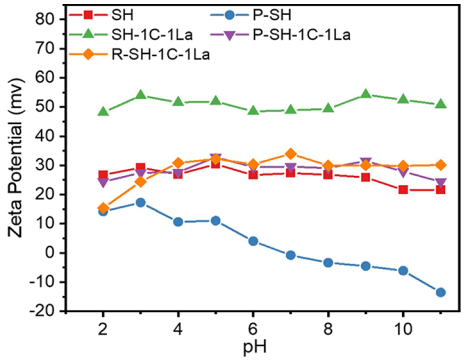

Figure 8. Zeta potential of SH, SH-C-La, P-SH, P-SH-C-La, and R-SH-1C-1La.

unchanged in the tested pH range (2.0∼11.0). SH-1C-1La exhibits zeta-potential values significantly higher than those of SH, indicating the modification by lanthanum oxalate improves the surface potential to strengthen the electrostatic interactions. This might help explain the excellent adsorption of SH-1C-1La in the high pH region.[51] After *P* adsorption, the zeta potential of SH and SH-1C-1La both decreases, which is consistent with the anion (e.g., phosphate) adsorption on the surface. The decrease in the zeta potential on SH-1C-1La may also be an indication of inner-sphere complexation.[52] It is interesting that after regeneration, the surface potential of R-SH-1C-1La is similar to that of P-SH-1C-1La and lower than that of the original SH-1C-1La. This observation may imply the transformation of lanthanum oxalate species during the regeneration process. Meanwhile, the decrease in the zeta potential could also explain the slightly decreased adsorption capacity of R-SH-1C-1La in comparison with SH-1C-1La.

However, it is worth pointing out that, for SH, the zeta potential is relatively stable across the whole pH range. Still, its high pH adsorption capacity is significantly lower. If the zeta potential is not the sole reason for adsorption enhancement, what else could it be?

To provide further insight into the adsorption mechanism of SH-1C-1La, XPS spectra are collected. Figure 9a shows the XPS survey spectra of SH-1C-1La and P-SH-1C-1La. The result clearly indicates the appearance of the P 2p signal (at 133.47 eV, see also Figure 9b) after *P* adsorption. The La XPS signal can be divided into La $3d_{5/2}$ and La $3d_{3/2}$, implying the existence of both bonding and antibonding states of La^{3+}.[32] Before the *P* adsorption, the La $3d_{5/2}$ signals are located at 836.0 and 839.14 eV, while the signals at 852.85 and 856.0 eV are assigned to La $3d_{3/2}$ (Figure 9c,d). These signals can all be attributed to the La−O bonding from lanthanum oxalate.[32] After *P* adsorption, the XPS signals of La shift to lower binding energy (Figure 9e,f). These results are consistent with the strong affinity between La and phosphate, forming La−O−P inner-sphere complexation.[37]

The XPS spectra are also collected on R-SH-1C-1La before and after the P adsorption (Figure S9). After regeneration, it is clear that the La $3d_{3/2}$ and $3d_{5/2}$ signals restore to the patterns similar to SH-1C-1La, confirming that the chemical interaction between La and P has disappeared. The similar binding energy indicates that lanthanum exists as oxalate species, but now nanocrystalline or amorphous, so could not be detected by XRD. Subsequently, after phosphate adsorption, new La−O−P inner-sphere complexation forms, revealing that La is still active for adsorbing phosphate ions although not in the form of bulk lanthanum oxalate. This again confirms the beneficial effect of lanthanum oxalate loading for the phosphate adsorption process.

Overall, the above results confirm that lanthanum oxalate species induce strong lanthanum-phosphate interactions (through chemisorption) while increasing the zeta potential, both of which are highly favorable for the phosphate interaction and therefore enhance the high pH adsorption of SH.

4. CONCLUSIONS

In this study, we synthesize a series of composite absorbents consisting of an amidocyanogen-rich polymer SH and lanthanum oxalate (SH-C-La). With less than 6 wt% in La content, this simple modification significantly increases the adsorption capacity of the SH matrix under alkaline conditions, with the maximum adsorption capacity of the SH-1C-1La being 109.3 mg P g^{-1} at pH 8.0 and 100.2 mg P g^{-1} at pH 10.0, respectively. Meanwhile, after four regeneration cycles, SH-1C-1La retains more than 78 and 85% of its original capacities at pH 8.0 and 10.0, respectively, showing its durability for long-time running. We find that the lanthanum oxalate species introduce strong lanthanum-phosphate interactions while increasing the zeta-potential of the SH-based adsorbents,

https://doi.org/10.1021/acsomega.2c01520
ACS Omega 2022, 7, 19743−19753

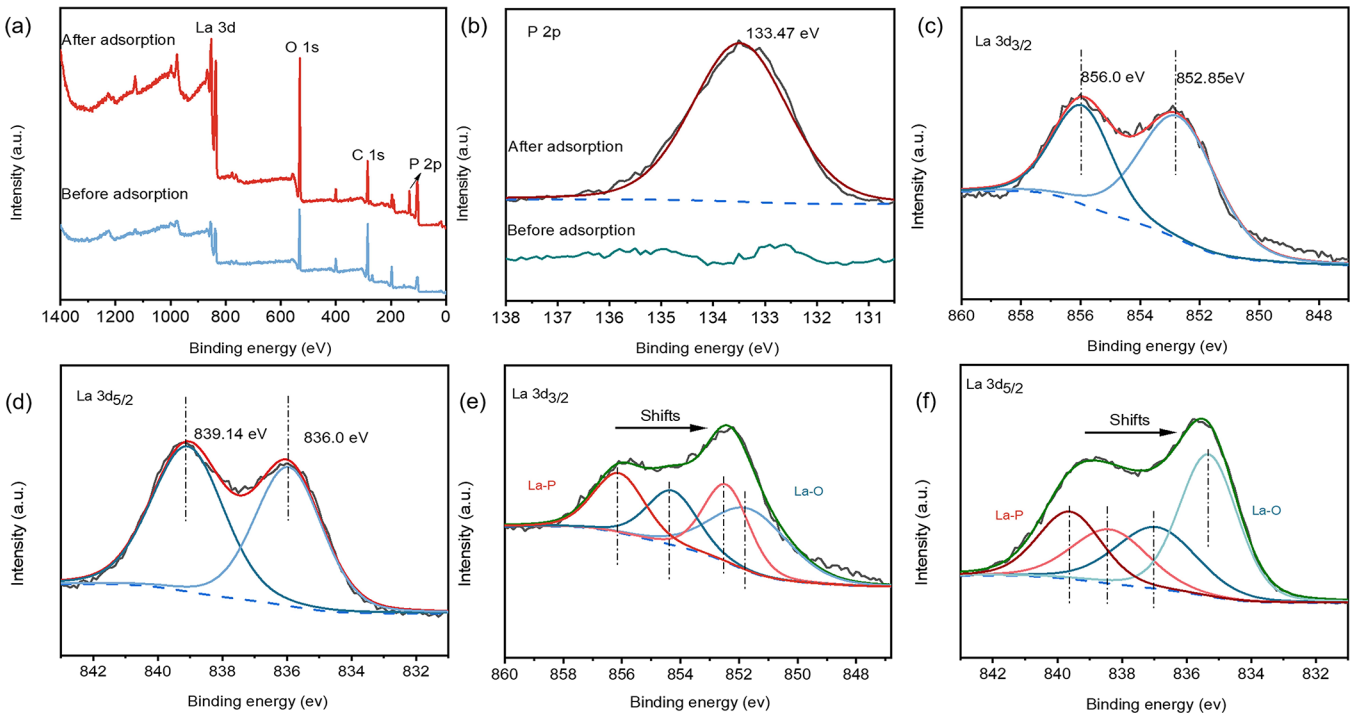

Figure 9. XPS spectra of SH-1C-1La and P-SH-1C-1La: survey spectra (a), P 2p spectrum (b), La $3d_{3/2}$ and La $3d_{5/2}$ spectra of SH-1C-1La (c,d), and La $3d_{3/2}$ and La $3d_{5/2}$ spectra of P-SH-1C-1La (e,f).

both of which contribute synergistically to enhance the phosphate adsorption at high pH. With improved adsorption capacity at high pH and excellent regeneration property, our results may provide an alternative for improving the adsorption behavior of anion-exchange resins via lanthanum oxalate loading.

Meanwhile, although SH-1C-1La might be worth considering for wastewater treatment, its significant swelling after soaking in water prevents us from evaluating the continuous column treatment capability. Further studies are required to minimize the swelling of resins, potentially via cross-linking modifications. In addition, we used a simulated wastewater with a high concentration of phosphate that does not exist in natural aqueous environment for this research.[53] Practical wastewater samples need to be used to further evaluate the feasibility of using SH-1C-1La in real-life conditions. These future work will be provided in our forthcoming contributions.

■ ASSOCIATED CONTENT

Supporting Information

The Supporting Information is available free of charge at https://pubs.acs.org/doi/10.1021/acsomega.2c01520.

La loading of various as-prepared SH-C-La (Table S1), regeneration efficiency of SH-1C-1La (Table S2), SEM images of SH, SH-1C-0.6La, SH-1C-1La, and SH-2.5C-1La (Figure S1), SEM image of La-oxalate (Figure S2), EDS image of SH-1C-1La (Figure S3), P adsorption capacities of SH in various pH (Figure S4), the ratio of adsorption capacity values between SH and SH-1C-1La (Figure S5), La% of SH-1C-1La and La% leaching after regeneration (Figure S6), SEM of P-SH-1C-1La (Figure S7), EDS image of samples after *P* adsorption and regeneration (Figure S8), and XPS spectra of R-SH-1C-1La (Figure S9) (PDF)

■ AUTHOR INFORMATION

Corresponding Authors

Xin Ye − *Key Laboratory of Urban Pollutant Conversion, Institute of Urban Environment, Chinese Academy of Sciences, Xiamen 361021, China;* orcid.org/0000-0003-2277-5328; Email: xye@iue.ac.cn

Wei Wang − *CAS Key Laboratory of Design and Assembly of Functional Nanostructures, and Fujian Provincial Key Laboratory of Nanomaterials, Fujian Institute of Research on the Structure of Matter, Chinese Academy of Sciences, Fuzhou 350002, China; Xiamen Institute of Rare Earth Materials, Haixi Institute, Chinese Academy of Sciences, Xiamen 361021, China;* orcid.org/0000-0003-3178-236X; Email: wangwei@fjirsm.ac.cn

Authors

Xiaofeng Xu − *College of Chemistry and Materials Science, Fujian Normal University, Fuzhou 350002, China; CAS Key Laboratory of Design and Assembly of Functional Nanostructures, and Fujian Provincial Key Laboratory of Nanomaterials, Fujian Institute of Research on the Structure of Matter, Chinese Academy of Sciences, Fuzhou 350002, China; Xiamen Institute of Rare Earth Materials, Haixi Institute, Chinese Academy of Sciences, Xiamen 361021, China*

Ruonan Li − *CAS Key Laboratory of Design and Assembly of Functional Nanostructures, and Fujian Provincial Key Laboratory of Nanomaterials, Fujian Institute of Research on the Structure of Matter, Chinese Academy of Sciences, Fuzhou 350002, China; Xiamen Institute of Rare Earth Materials, Haixi Institute, Chinese Academy of Sciences, Xiamen 361021, China*

Jinglin Chen − *Key Laboratory of Urban Pollutant Conversion, Institute of Urban Environment, Chinese Academy of Sciences, Xiamen 361021, China*

https://doi.org/10.1021/acsomega.2c01520
ACS Omega 2022, 7, 19743−19753

Jie Yang − *College of Chemistry and Materials Science, Fujian Normal University, Fuzhou 350002, China; CAS Key Laboratory of Design and Assembly of Functional Nanostructures, and Fujian Provincial Key Laboratory of Nanomaterials, Fujian Institute of Research on the Structure of Matter, Chinese Academy of Sciences, Fuzhou 350002, China; Xiamen Institute of Rare Earth Materials, Haixi Institute, Chinese Academy of Sciences, Xiamen 361021, China*

Yukai Wu − *Key Laboratory of Urban Pollutant Conversion, Institute of Urban Environment, Chinese Academy of Sciences, Xiamen 361021, China*

Junrui Liu − *College of Chemistry and Materials Science, Fujian Normal University, Fuzhou 350002, China; CAS Key Laboratory of Design and Assembly of Functional Nanostructures, and Fujian Provincial Key Laboratory of Nanomaterials, Fujian Institute of Research on the Structure of Matter, Chinese Academy of Sciences, Fuzhou 350002, China; Xiamen Institute of Rare Earth Materials, Haixi Institute, Chinese Academy of Sciences, Xiamen 361021, China*

You-gui Huang − *CAS Key Laboratory of Design and Assembly of Functional Nanostructures, and Fujian Provincial Key Laboratory of Nanomaterials, Fujian Institute of Research on the Structure of Matter, Chinese Academy of Sciences, Fuzhou 350002, China; Xiamen Institute of Rare Earth Materials, Haixi Institute, Chinese Academy of Sciences, Xiamen 361021, China;* orcid.org/0000-0001-9962-3723

Shaohua Chen − *Key Laboratory of Urban Pollutant Conversion, Institute of Urban Environment, Chinese Academy of Sciences, Xiamen 361021, China*

Complete contact information is available at: https://pubs.acs.org/10.1021/acsomega.2c01520

Notes

The authors declare no competing financial interest.

■ ACKNOWLEDGMENTS

We thank the financial support from the Youth Innovation Promotion Association CAS (No. 2021302 and No. 2021305) and the FJIRSM&IUE Joint Research Fund (No. RHZX-2019-003).

■ REFERENCES

(1) Ekholm, P.; Krogerus, K. Bioavailability of phosphorus in purified municipal wastewaters. *Water Res.* **1998**, *32*, 343−351.
(2) Correll, D. L. The role of phosphorus in the eutrophication of receiving waters: a review. *J. Environ. Qual.* **1998**, *27*, 261−266.
(3) Zhang, P. Comprehensive recovery and sustainable development of phosphate resources. *Procedia Eng.* **2014**, *83*, 37−51.
(4) Kumar, P. S.; Korving, L.; van Loosdrecht, M. C. M.; Witkamp, G. J. Adsorption as a technology to achieve ultra-low concentrations of phosphate: Research gaps and economic analysis. *Water Res. X* **2019**, *4*, No. 100029.
(5) Zhang, Y.; Pan, B.; Shan, C.; Gao, X. Enhanced phosphate removal by nanosized hydrated La(III) oxide confined in cross-linked polystyrene networks. *Environ. Sci. Technol.* **2016**, *50*, 1447−1454.
(6) Stefoni, S.; Feliciangeli, G.; Cianciolo, G.; Sanctis, L.; Spighi, M. Hemoperfusion in chronic uremia. *Boll. Soc. Ital. Biol. Sper.* **1993**, *69*, 675−682.
(7) Golden, L. S. Ion Exchange resins: characterization of. *Encyclopedia of Separation Science*; Elsevier Science Ltd., 2000; Vol. 33, pp 3172−3179.
(8) Pan, B.; Wu, J.; Pan, B.; Lv, L.; Zhang, W.; Xiao, L.; Wang, X.; Tao, X.; Zheng, S. Development of polymer-based nanosized hydrated ferric oxides (HFOs) for enhanced phosphate removal from waste effluents. *Water Res.* **2009**, *43*, 4421−4429.
(9) Chen, L.; Zhao, X.; Pan, B.; Zhang, W.; Hua, M.; Lv, L.; Zhang, W. Preferable removal of phosphate from water using hydrous zirconium oxide-based nanocomposite of high stability. *J. Hazard. Mater.* **2015**, *284*, 35−42.
(10) Holmes-Farley, S. R.; Mandeville, W. H.; Ward, J.; Miller, K. L. Design and characterization of sevelamer hydrochloride: a novel phosphate-binding pharmaceutical. *J. Macromol. Sci., Part A: Pure Appl.Chem.* **1999**, *36*, 1085−1091.
(11) Wrong, O.; Harland, C. Sevelamer and other anion-exchange resins in the prevention and treatment of hyperphosphataemia in chronic renal failure. *Nephron Physiol.* **2007**, *107*, 17−33.
(12) Zang, Y.; Yue, Q.; Kan, Y.; Zhang, L.; Gao, B. Research on adsorption of Cr(VI) by Poly-epichlorohydrin-dimethylamine (EPI-DMA) modified weakly basic anion-exchange resin D301. *Ecotoxicol. Environ. Saf.* **2018**, *161*, 467−473.
(13) Goodman, W. G.; Goldin, J.; Kuizon, B. D.; Yoon, C.; Salusky, I. B. Coronary-artery calcification in young adults with end-stage renal disease who are undergoing dialysis. *N. Engl. J. Med.* **2000**, *342*, 1478−1483.
(14) Elsiddig, R.; Hughes, H.; Owens, E.; O'Reilly, N. J.; O'Grady, D.; McLoughlin, P. Kinetic and thermodynamic evaluation of phosphate ions binding onto sevelamer hydrochloride. *Int. J. Pharm.* **2014**, *474*, 25−32.
(15) Hudson, S. P.; Owens, E.; Hughes, H.; McLoughlin, P. Enhancement and restriction of chain motion in polymer networks. *Int. J. Pharm.* **2012**, *430*, 34−41.
(16) Wang, Z.; Yi, C.; Ren, A.; Tuo, Y.; Zhang, F.; Wang, Y. The invention relates to a nicotinic acid sviram and a preparation method and application thereof. CN102993348A, 2014.
(17) Chen, X.; Su, X.; Dai, J.; Wang, J. A synthetic method of sviram carbonate. CN108440697A, 2018.
(18) Chen, D.; Yu, H.; Pan, M.; Pan, B. Hydrogen bonding-orientated selectivity of phosphate adsorption by imine-functionalized adsorbent. *Chem. Eng. J.* **2021**, *433*, No. 133690.
(19) Kunhikrishnan, A.; Rahman, M. A.; Lamb, D.; Bolan, N. S.; Saggar, S.; Surapaneni, A.; Chen, C. Rare earth elements (REE) for the removal and recovery of phosphorus: A review. *Chemosphere* **2022**, *286*, No. 131661.
(20) Wu, B.; Wan, J.; Zhang, Y.; Pan, B.; Lo, I. M. C. Selective phosphate removal from water and wastewater using sorption: process fundamentals and removal mechanisms. *Environ. Sci. Technol.* **2020**, *54*, 50−66.
(21) Dong, S.; Wang, Y.; Zhao, Y.; Zhou, X.; Zheng, H. La^{3+}/$La(OH)_3$ loaded magnetic cationic hydrogel composites for phosphate removal: Effect of lanthanum species and mechanistic study. *Water Res.* **2017**, *126*, 433−441.
(22) Park, Y.; Gorman, C.; Ford, E. Lanthanum carbonate nanofibers for phosphorus removal from water. *J. Mater. Sci.* **2020**, *55*, 5008−5020.
(23) Zong, E.; Liu, X.; Wang, J.; Yang, S.; Jiang, J.; Fu, S. Facile preparation and characterization of lanthanum-loaded carboxylated multi-walled carbon nanotubes and their application for the adsorption of phosphate ions. *J. Mater. Sci.* **2017**, *52*, 7294−7310.
(24) Liao, T.; Li, T.; Su, X.; Yu, X.; Song, H.; Zhu, Y.; Zhang, Y. $La(OH)_3$-modified magnetic pineapple biochar as novel adsorbents for efficient phosphate removal. *Bioresour. Technol.* **2018**, *263*, 207−213.
(25) Tang, Q.; Shi, C.; Shi, W.; Huang, X.; Ye, Y.; Jiang, W.; Kang, J.; Liu, D.; Ren, Y.; Li, D. Preferable phosphate removal by nano-La(III) hydroxides modified mesoporous rice husk biochars: Role of the host pore structure and point of zero charge. *Sci. Total Environ.* **2019**, *662*, 511−520.
(26) Su, C.; Puls, R. W. Arsenate and arsenite removal by zerovalent iron: effects of phosphate, silicate, carbonate, borate, sulfate,

chromate, molybdate, and nitrate, relative to chloride. *Environ. Sci. Technol.* **2001**, *35*, 4562−4568.
(27) Chall, S.; Pramanik, S.; Dhar, S.; Saha, A.; Bhattacharya, S. C. Facile room temperature synthesis of lanthanum oxalate nanorods and their interaction with antioxidative naphthalimide derivative. *J. Nanosci. Nanotechnol.* **2012**, *12*, 2229−2238.
(28) Zhang, Y.; Zhu, W.; He, H.; Zheng, A. Synthesis of lanthanum oxalate hierarchical micro-particles and nano-tubes. *J. Exp. Nanosci.* **2012**, *9*, 851−859.
(29) Alenazi, N.; Hussein, M.; Alamry, K.; Asiri, A. Nanocomposite-based aminated polyethersulfone and carboxylate activated carbon for environmental application. A real sample analysis. *C* **2018**, *4*, 30.
(30) Ma, M.; Li, H.; Yang, W.; Wu, Q.; Shi, D.; Zhao, Y.; Feng, C.; Jiao, Q. Polystyrene nanometer-sized particles supported alkaline imidazolium ionic liquids as reusable and efficient catalysts for the knoevenagel condensation in aqueous phase. *Catal. Lett.* **2017**, *148*, 134−143.
(31) Baker, P.; Smith, A. Structure of lanthanum chloride oxalate trihydrate. *Acta Crystallogr., Sect. A: Found. Crystallogr.* **1990**, *46*, 984−985.
(32) Prabhu, S. M.; Chuaicham, C.; Sasaki, K. A mechanistic approach for the synthesis of carboxylate-rich carbonaceous biomass-doped Lanthanum-oxalate nanocomplex for arsenate adsorption. *ACS Sustainable Chem. Eng.* **2018**, *6*, 6052−6063.
(33) Zhang, L.; He, F.; Mao, W.; Guan, Y. Fast and efficient removal of Cr(VI) to ppb level together with Cr(III) sequestration in water using layered double hydroxide interclated with diethyldithiocarbamate. *Sci. Total Environ.* **2020**, *727*, No. 138701.
(34) Dithmer, L.; Nielsen, U. G.; Lundberg, D.; Reitzel, K. Influence of dissolved organic carbon on the efficiency of P sequestration by a lanthanum modified clay. *Water Res.* **2016**, *97*, 39−46.
(35) Pechenyuk, S. I.; Semushina, Y. P.; Kuz' mich, L. F. Adsorption affinity of anions on metal oxyhydroxides. *Russ. J. Phys. Chem. A* **2013**, *87*, 490−496.
(36) Foo, K. Y.; Hameed, B. H. Insights into the modeling of adsorption isotherm systems. *Chem. Eng. J.* **2010**, *156*, 2−10.
(37) Wu, Y.; Li, X.; Yang, Q.; Wang, D.; Xu, Q.; Yao, F.; Chen, F.; Tao, Z.; Huang, X. Hydrated lanthanum oxide-modified diatomite as highly efficient adsorbent for low-concentration phosphate removal from secondary effluents. *J. Environ. Manage.* **2019**, *231*, 370−379.
(38) Desta, M. B. Batch sorption experiments: Langmuir and Freundlich isotherm studies for the adsorption of textile metal ions onto teff straw (Eragrostis tef) agricultural waste. *J. Thermodyn.* **2013**, *2013*, 1−6.
(39) Hameed, B. H.; Din, A. T.; Ahmad, A. L. Adsorption of methylene blue onto bamboo-based activated carbon: kinetics and equilibrium studies. *J. Hazard. Mater.* **2007**, *141*, 819−825.
(40) Ho, Y. S.; McKay, G. A comparison of chemisorption kinetic models applied to pollutant removal on various sorbents. *Process Saf. Environ. Prot.* **1998**, *76*, 332−340.
(41) Tan, K. L.; Hameed, B. H. Insight into the adsorption kinetics models for the removal of contaminants from aqueous solutions. *J. Taiwan Inst. Chem. Eng.* **2017**, *74*, 25−48.
(42) Revellame, E. D.; Fortela, D. L.; Sharp, W.; Hernandez, R. Adsorption kinetic modeling using pseudo-first order and pseudo-second order rate laws: A review. *Clean. Eng. Technol.* **2020**, *1*, No. 100032.
(43) Kumar, P. S.; Ejerssa, W. W.; Wegener, C. C.; Korving, L.; Dugulan, A. I.; Temmink, H.; van Loosdrecht, M. C. M.; Witkamp, G. J. Understanding and improving the reusability of phosphate adsorbents for wastewater effluent polishing. *Water Res.* **2018**, *145*, 365−374.
(44) Vakili, M.; Deng, S.; Cagnetta, G.; Wang, W.; Meng, P.; Liu, D.; Yu, G. Regeneration of chitosan-based adsorbents used in heavy metal adsorption: A review. *Sep. Purif. Technol.* **2019**, *224*, 373−387.
(45) Bhatti, J. S.; Comerford, N. B.; Johnston, C. T. Influence of oxalate and soil organic matter on sorption and desorption of phosphate onto a spodic horizon. *Soil Sci. Soc. Am. J.* **1998**, *62*, 1089−1095.
(46) Liu, F.; De Cristofaro, A.; Violante, A. Effect of pH, Phosphate and oxalate on the adsorption/desorption of arsenate on/from goethite. *Soil Sci.* **2001**, *166*, 197−208.
(47) Wang, X.; Zhang, L.; Zhang, Z.; Wang, X. Effects of pH value on growth morphology of $LaPO_4$ nanocrystals: investigated from experiment and theoretical calculations. *Appl. Phys. A: Mater. Sci. Process.* **2016**, *122*, 508.
(48) Li, L.; Jiang, W.; Pan, H.; Xu, X.; Tang, Y.; Ming, J.; Xu, Z.; Tang, R. Improved luminescence of Lanthanide(III)-Doped nanophosphors by linear aggregation. *J. Phys. Chem. C* **2008**, *111*, 4111−4115.
(49) Kirchner, B.; Spickermann, C.; Reckien, W.; Schalley, C. A. Uncovering individual hydrogen bonds in rotaxanes by frequency shifts. *J. Am. Chem. Soc.* **2010**, *132*, 484−494.
(50) Tadi, K. K.; Motghare, R. V. Computational and experimental studies on oxalic acid imprinted polymer. *J. Chem. Sci.* **2013**, *125*, 413−418.
(51) Koilraj, P.; Sasaki, K. Selective removal of phosphate using La-porous carbon composites from aqueous solutions: Batch and column studies. *Chem. Eng. J.* **2017**, *317*, 1059−1068.
(52) Yang, Y.; Wang, Y.; Zheng, C.; Lin, H.; Xu, R.; Zhu, H.; Bao, L.; Xu, X. Lanthanum carbonate grafted ZSM-5 for superior phosphate uptake: Investigation of the growth and adsorption mechanism. *Chem. Eng. J.* **2022**, *430*, No. 133166.
(53) Cai, W.; Chang, C.; Song, S.; Li, J.; Zhang, F.; Li, F. Spatial distribution and sources of groundwater phosphorus in Dezhou Region. *Chin. J. Eco-Agric.* **2013**, *21*, 456−464.

https://doi.org/10.1021/acsomega.2c01520
ACS Omega 2022, 7, 19743−19753